The current issue and full text archive of this journal is available at
www.emeraldinsight.com/0961-5539.htm

Analysis of pressure field in time domain using nonlinear reduced frequency approach in unsteady transonic flows

M. Kharati Koopaee, M.M. Alishahi and H. Emdad
Department of Mechanical Engineering, Shiraz University, Shiraz, Iran

Received 27 March 2009
Accepted 10 September 2009

Abstract

Purpose – The purpose of this paper is to discuss the capability of nonlinear frequency domain (NLFD) method in predicting surface pressure coefficient presented in the time domain in unsteady transonic flows.

Design/methodology/approach – In this research, the solution and spatial operator are approximated by discrete form of Fourier transformation and resulting nonlinear equations are solved by use of pseudo-spectral approach. Considered transonic flows involve different flow pattern on the airfoil surfaces. One of the test cases involves moving shocks on both lower and upper airfoil surfaces and in the two other test cases a moving shock occurs only on the upper surface.

Findings – Pressure distributions presented in the time domain using NLFD are compared with three test cases. Results show that NLFD predicts reasonable pressure distributions in time domain except in vicinity of shock positions. Although this method may predict unfair results near shock positions, however gives good estimates for global properties such as lift coefficient.

Originality/value – In the previous works on NLFD method, the flow field results have been limited to representing the pressure in the frequency domain or global coefficients such as lift coefficients. No details of pressure distributions in the time domain have been provided in such investigations. In this research, by presenting the pressure in the time domain, the conditions on which good pressure distributions are obtained are demonstrated.

Keywords Flow, Air, Pressure, Aircraft

Paper type Research paper

1. Introduction

The calculation of unsteady flows continues to challenge computational fluid dynamists (CFD). This challenge comes from the fact that in addition to preserving the accurate spatial discretization for steady-state solutions, unsteady codes should also accurately resolve the time history of the solution. The challenge to CFD lies in this added dimension and its associated computational cost.

The time accurate methods are common ones in solving unsteady flows. These methods include explicit and implicit time stepping schemes and factored ADI. Although these methods are applicable to a wide range of unsteady flows, they consume more computational time than steady-state solvers. In these methods, the semi-discrete form of governing equations is constructed by discretizing the space while leaving the time term. Finally, advancing in time leads to the solution.

An alternative to the time accurate methods is to assume a periodic solution over a time interval regarding the fact that transient portion of solution is of less importance. Examples of such solutions are among unsteady flows in turbomachinery cascades. Given the assumption of periodicity, some special methods can be used to calculate the solution. It is evident that the transient decay of the solution using these methods cannot be admitted as a part of the solution.

International Journal of Numerical Methods for Heat & Fluid Flow
Vol. 20 No. 6, 2010
pp. 655-669

0961-5539
DOI 10.1108/09615531011056818

A less computationally expensive approach for these unsteady flows is to linearize the flow field about a mean flow solution (Ni and Sisto, 1976; Hall and Crawley, 1989; Clark, 1992; Holmes and Chuang, 1993; Hall and Lorence, 1993; Hall and Clark, 1993; Hall *et al.*, 1994). Assuming small unsteady variations, the flow may be decomposed into two parts: a nonlinear steady or mean flow, plus a linear small perturbation flow. In general, the steady flow is described by a set of nonlinear partial differential equations, whereas the unsteady small perturbation flow is described by a set of linear variable coefficient partial differential equations that by adding pseudo time term become hyperbolic in time. Because the unsteady perturbation flow is periodic in time, we may, without loss of generality, represent the unsteady flow as a Fourier series in time with coefficients that vary spatially. Each Fourier coefficient is described by a set of partial differential equations. If any unsteadiness in the flow is harmonic in time, it can be represented as $ue^{i\omega t}$, where u is complex amplitude of unsteady variable, i is imaginary number ($\sqrt{-1}$) and ω is the frequency of unsteady disturbances, then the time derivatives $\partial/\partial t$ are replaced by $i\omega$, so that time does not appear explicitly.

To reduce the error associated with the linearized form of reduced frequency approach, nonlinear form of this approach can be used. A number of investigators have developed frequency domain analysis of nonlinear unsteady flows (Adamczyk, 1984; Ning and He, 1998; Thomas *et al.*, 2002). Adamczyk (1984) proposed several different linearizations and averaging operators of the velocity variable to form what he termed the deterministic stress. This term is similar to the Reynolds stress in that it attempts to quantify the effects of the unsteady field on the time averaged solution. Adamczyk (1984) proposed such a modeling for these terms (McMullen, 2003). Ning and He (1998) used averaging operators to determine the deterministic stress. They proposed calculating these terms with a modified version of a linearized frequency domain solver. While the methods differ somewhat in details, most of them can be viewed as a form of harmonic balance. Although some of the nonlinear effects are addressed in these methods, the higher order terms are still neglected in the solution of unsteady modes. The assumptions of the linearization still must apply for these modes, therefore limiting the applicability of these methods.

None of the preceding methods can adequately account for the strong nonlinearities. This brings us to methods which represent the full nonlinear equations in the frequency domain. Efficient periodic solutions to full nonlinear systems of equations were first proposed by Hall *et al.* (2000, 2002) using the harmonic balance technique on two-dimensional (2-D) turbomachinery cascades. This technique utilizes a pseudo-spectral approach to represent the nonlinear residual in the temporal domain (McMullen and Jameson, 2006). McMullen *et al.* (2001, 2002) proposed the nonlinear frequency domain method which represents a form of the residual in the frequency domain. They also focused on 2-D turbomachinery flows. Regardless of the approach, iterative methods were then employed to drive this residual to a negligible value in a manner that is consistent with steady-state solvers. They have demonstrated the efficiency of this technique to represent complex nonlinear flow solutions using a minimum number of modes. If all the modes of the solution converge as quickly as a similar steady-state calculation, then the cost of the calculation is the product of the cost of a steady solution and the number of instances used in the time series of the unsteady residual. This is consistent with linearized methods except that a slight penalty is incurred by the additional memory required to hold all the unsteady modes simultaneously.

In previous reduced frequency studies, normally the flow field results were presented in terms of pressure distributions in the frequency domain or integrated

coefficients such as lift coefficients. No details of pressure distributions in the time domain were provided in such investigations. This deficiency together with the question of how well nonlinear effects in the time domain can be modeled in a nonlinear frequency domain (NLFD) approach provided the aims of this study.

2. Governing equations

For an arbitrary volume of fluid, governing equations in integral form can be expressed as:

$$\frac{d}{dt}\int_V \vec{W}dV + \int_S \vec{F}\cdot\vec{N}ds = 0 \tag{1}$$

In this equation, $\int_V \vec{W}dV$ and $\int_S \vec{F}\cdot\vec{N}ds$ are volumetric integrals of the state vector and surface integrals of fluxes, respectively. $\vec{N}$ is also normal unit vectors pointed outward for the considered volume. In two dimensions, the state vector comprises physical properties of fluid (density ρ, Cartesian velocity component u_i and stagnation energy E) and can be expressed as the following vector:

$$\vec{W} = \begin{bmatrix} \rho \\ \rho u_1 \\ \rho u_2 \\ \rho E \end{bmatrix} \tag{2}$$

The flux vector includes transport of these properties and those terms associated with a moving control volume. If the velocity of control volume surfaces is denoted as $\vec{b}$, for each direction, i, the flux vector for a 2-D flow can be expressed as:

$$F_i = \begin{bmatrix} \rho(u_i - b_i) \\ \rho u_1(u_i - b_i) + \delta_{1i}p \\ \rho u_2(u_i - b_i) + \delta_{2i}p \\ \rho E(u_i - b_i) + u_i p \end{bmatrix} \tag{3}$$

where δ_{ij} is the Kronecker delta.

3. Transforming the equations into the frequency domain

The technique used in this study is the finite volume approach where the continuous surface integrals are represented by a discrete summation of fluxes across a finite number of faces on the control volume:

$$\int_S \vec{F}\cdot\vec{N}ds = \sum_{cs}\vec{F}\cdot\vec{S} \tag{4}$$

Having approximated all the spatial operators, the remaining term in the conservation laws is the temporal derivative of the volumetric integral of the solution. This is approximated as the product of the cell volume, V, with the temporal derivative of the average of the solution over the cell. Adding the spatial and temporal operators together results in the complete approximation to the governing equations:

$$V\frac{\partial W}{\partial t}+\sum_{cv}\vec{F}\cdot\vec{S}=0 \tag{5}$$

The spatial operator R is introduced as a function of space and time including both the convective and artificial dissipation fluxes, F_d, provided by shock capturing schemes:

$$R=\sum_{cv}\vec{F}\cdot\vec{S}+F_d \tag{6}$$

In this research, Jameson scheme is used for artificial dissipation fluxes. Taking advantage of this simplified notation, a semi-discrete form of the governing equations can be written as:

$$V\frac{\partial W}{\partial t}+R=0 \tag{7}$$

Assuming that the solution W and spatial operator R are periodic in time, both can be represented by separate Fourier series:

$$W=\sum_{k=-\left(\frac{N-1}{2}\right)}^{k=\left(\frac{N-1}{2}\right)}\hat{W}_k e^{ik\omega t} \tag{8}$$

$$R=\sum_{k=-\left(\frac{N-1}{2}\right)}^{k=\left(\frac{N-1}{2}\right)}\hat{R}_k e^{ik\omega t} \tag{9}$$

These discrete Fourier transforms can be substituted into the semi-discrete form of the governing equations (7), and the time derivative of the state variable can be moved inside the series summation. Taking advantage of the orthogonality of the Fourier terms a separate equation for each wave number, k, is obtained:

$$ikV\omega\hat{W}_k+\hat{R}_k=0 \tag{10}$$

However, each coefficient $\hat{R}_k$ of the transformation of the residual depends on all coefficients of $\hat{W}_k$, because $R(W(t))$ is a nonlinear function of $W(t)$. Thus Equation (10) represents a nonlinear set of equations which must be solved iteratively. The solver attempts to find a solution, W, that drives this system of equations to zero for all wave numbers, but at any iteration in the solution process the unsteady residual, $\hat{I}_k$, will be finite (McMullen, 2003):

$$\hat{I}_k=ikV\omega\hat{W}_k+\hat{R}_k \tag{11}$$

4. Solution procedure

The nonlinearity of the unsteady residual stems from the spatial operator. There are two approaches for calculating the spatial operator expressed in the frequency domain. The first uses a complex series of convolution sums to calculate $\hat{R}_k$ directly from $\hat{W}_k$.

Such an approach was discussed in Hall's introductory paper (Hall *et al.*, 2000) on harmonic balance techniques. Hall justly discarded the approach due to its massive complexity (considering artificial dissipation schemes and turbulence modeling) and the cost that scales quadratically with the number of modes N (McMullen, 2003).

The alternative proposed by Hall with some implementations by McMullen (2003) is to use a pseudo-spectral approach that relies on the computational efficiency of the fast Fourier transform (FFT). A diagram detailing the transformations used by the pseudo-spectral approach is provided in Figure 1.

The pseudo-spectral approach begins by assuming that $\hat{W}_k$ is known for all wave numbers. Using an inverse FFT, $\hat{W}_k$ can be transformed back to the physical space resulting in a state vector $W(t)$ sampled at evenly distributed intervals over the time period. At each of these time instances the steady-state operator $R(W(t))$ can be computed. An FFT is then used to transform the spatial operator to the frequency domain where $\hat{R}_k$ is known for all wave numbers. The unsteady residual $\hat{I}_k$ can then be calculated by adding $\hat{R}_k$ to the spectral representation of the temporal derivative $ikV\omega\hat{W}_k$ (McMullen, 2003). Advancing in pseudo time is stopped when unsteady residual $\hat{I}_k$ reaches to a desirable minimum value. Since $\hat{W}_k$ are known for all wave numbers, transforming back to the physical space using Equation (8) at a given time instance leads to the solution W at that instance. Thus, pressure coefficient can be calculated at the given time instance.

The cost of evaluating the spatial operator is the product of the cost of evaluating a steady-state spatial operator and the number of time instances used to represent the solution N. The cost of the FFT is proportional to $N\ln(N)$. For most realistic values of N ($N = 1 \rightarrow 10$) the cost of the pseudo-spectral approach is determined by the cost associated with calculating the spatial operator (McMullen, 2003).

One of the advantages of the pseudo-spectral approach is its flexibility in admitting different forms of the nonlinear operators. Although this research will use finite volume formulations, the application of the pseudo-spectral approach is equally well suited for finite difference or other types of spatial operators (McMullen, 2003).

5. Boundary conditions

Boundary conditions are applied by introducing ghost cells near wall and the cells adjacent to the farfield. The density at the ghost cell near wall is set to be equal to the cell value adjacent to the wall.

Since inviscid flow solutions are studied, no flow across the wall is allowed. This requires the condition $(\vec{V}_w - \vec{V}_b) \,.\, \hat{n} = 0$ to be satisfied at the wall, where $\vec{V}_w$ and $\vec{V}_b$ denote flow velocity at the wall and the body velocity, respectively. $\hat{n}$ is normal unit vector pointed outward the wall. Therefore, velocity components in the ghost cells near wall are computed as follows:

$$\vec{V}_g = \vec{V}_{i,j} - 2\,[\,(\vec{V}_{i,j} - \vec{V}_b) \,.\, \hat{n}\,]\,\hat{n} \tag{12}$$

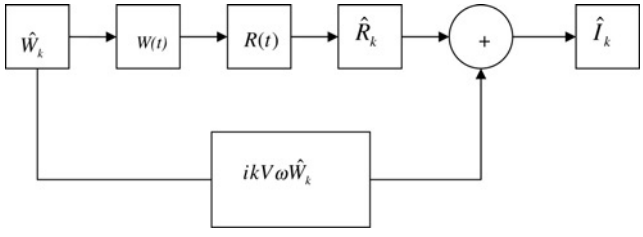

Figure 1.
Simplified dataflow diagram of the time advancement scheme illustrating the pseudo-spectral approach used in calculating the nonlinear spatial operator R

In this equation $\vec{V}_{i,j}$ is flow velocity in the cell adjacent to the wall.

The pressure in the ghost cells near wall is evaluated from the interior cells values considering wall acceleration. Thus, ghost cells pressure is calculated by simple discritization of the following equation:

$$\frac{\partial P}{\partial n} = -\rho \vec{a}_W \cdot \vec{n} \tag{13}$$

where $\vec{a}_W$ is the wall acceleration.

Boundary conditions in the ghost cells near farfield are also determined based on Riemann invariants applied to the farfield boundaries. To do this, the coordinate frame for the Riemann invariants is chosen along the pointing normal to the cell face and conservation of mass and momentum equations for one-dimensional flow along this direction are simplified into a system of material derivatives. Therefore, combinations of invariants according to the right and left running characteristics will lead to the boundary values for the problem.

6. Test case description

In this paper, NLFD results are compared with other results for three different cases. Two of them are associated with Landon's experiments as part of AGARD report (Landon, 2000). The third case is related to the results obtained from a finite-volume-based commercial CFD software. In this case, response to a forced oscillation of an airfoil is calculated.

In all cases mentioned above, airfoil is pitching about its quarter chord and its incidence is changed with time as the following:

$$\alpha = \alpha_m + \alpha_0 \,\mathrm{Sin}(\omega t) \tag{14}$$

α_m and α_0 are mean incidence and pitch amplitude, respectively. ω is the angular frequency and is given by:

$$\omega = 2\,k\,V_\infty / C \tag{15}$$

where k is the reduced frequency, V_∞ is the free-stream velocity and C is the chord length.

Important parameters of AGARD test cases are summarized in Table I.

While incidence angle increases in CT1 AGARD case, a shock wave appears on the upper surface and there is no shock wave on the lower surface (Uygun and Kirkkopru, 2007). In CT5 AGARD case, while airfoil is pitching, shock waves appear on the lower and upper airfoil surfaces in succession (Uygun and Kirkkopru, 2007).

Table I. Important parameters of AGARD test cases

Description	Variable	AGARD test case; CT1	AGARD test case; CT5
Mean angle of attack (deg)	α_m	2.89	0.016
Pitch amplitude (deg)	α_0	2.41	2.51
Reynolds number	R_{e_∞}	4.8×10^6	5.5×10^6
Mach number	M_∞	0.6	0.755
Reduced frequency	k	0.0808	0.0814

Unstructured triangular mesh is used to calculate the response to the forced oscillation in the CFD software. In this case, the grid used for calculation of the flow field at different time instances is generated by the software. This mesh topology is dictated due to software restriction in domain remeshing in each time steps. Table II indicates parameters of this chosen case.

Two different mesh sizes for mesh independency study of this case are considered. Table III presents their characteristics.

Figure 2 depicts the grid with 17,740 cells.

Mesh independency for the third case is studied comparing the results obtained by the software. Figure 3 presents pressure distribution as incidence angle reaches its maximum value, that is, 3°. Results show that there are little differences between these two mesh sizes. So, the mesh sized with 17,740 cells is used for comparison of results with NLFD results.

7. Pitching airfoil description

In this paper, three different girds of C-mesh topology are used for NLFD calculations. Table IV provides their defining characteristics.

Description	Variable	Third test case
Mean angle of attack (deg)	α_m	1.5
Pitch amplitude (deg)	α_0	1.5
Mach number	M_∞	0.7
Reduced frequency	k	0.1

Table II. Parameters of the third case

Number of triangular cells	Mean boundary distance (unit chord)	Number of grid points on the airfoil surface
17,740	22	490
30,498	22	614

Table III. Different mesh characteristics of the third case

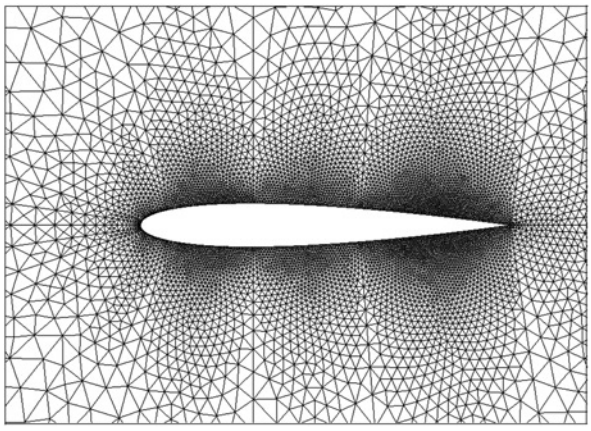

Figure 2. Nearfield picture of unstructured grid with 17,740 cells

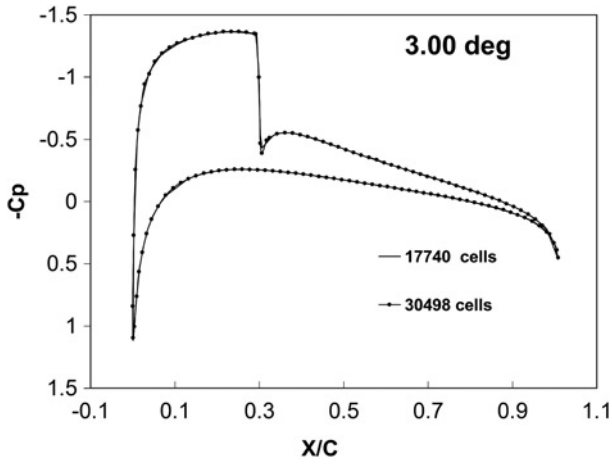

Figure 3.
Pressure distribution on the airfoil surfaces using two mesh sizes for the third case

Dimensions	Mean boundary distance (unit chord)	Mean grid spacing at wall (unit chord)	Number of grid points on the airfoil surface
31 × 299	22	0.0036	251
47 × 365	22	0.0026	297
61 × 385	22	0.0016	317

Table IV.
Description of meshes employed for NLFD calculations

Figure 4 provides a nearfield picture of grid dimensioned by 47 × 365.

8. Computational results and discussion

Grid independency of NLFD results is studied at arbitrary time instances for different test cases. This study for the CT1 and CT5 test cases has been done at 4.56 and 2.34°, respectively, while the airfoil pitches up. Grid study for the third case is at 3°. Figures 5-7 indicate the results using three, five and seven harmonics. These results show the

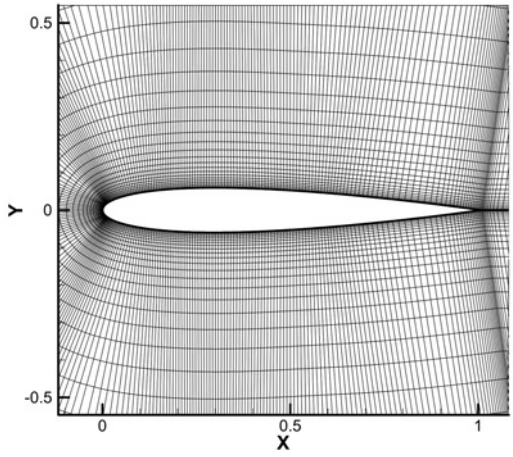

Figure 4.
Nearfield picture of grid dimensioned by 47 × 365

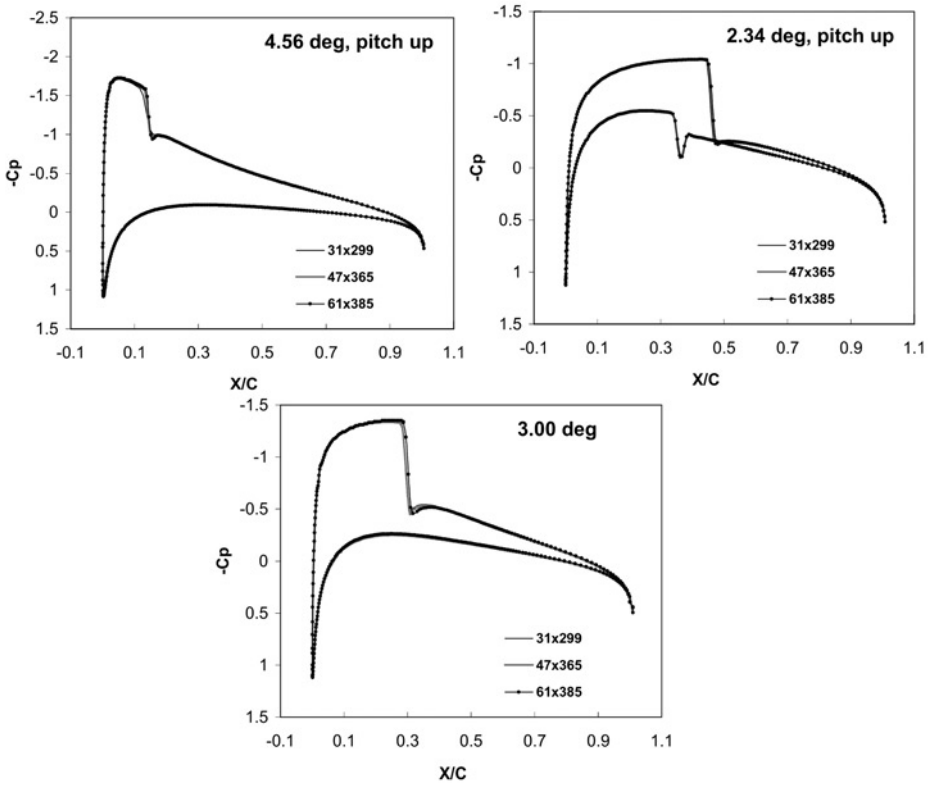

Figure 5.
Grid study for CT1 (top left), CT5 (top right) and the third (bottom) test case using three harmonics

grid with 47 × 365 cells has adequate grid density to be used for calculation. All results shown from now on are related to this grid type.

Figures 8 and 9 present pressure distribution at various time instances for CT1 and CT5 test cases, respectively. Experimental results are also included. As mentioned earlier, a moving shock appears on the upper and no moving shock occurs on the lower airfoil surface in CT1 test case while CT5 test case involves moving shocks on both airfoil surfaces. As can be seen, NLFD can predict fair pressure coefficient in CT1 test case on the lower and unfair pressure distribution around the positions in which shock appears in its periodic motion on the upper surface. There are also little differences between pressure coefficients on the lower surface using three, five and seven harmonics. In CT5 test case, which involves moving shocks on both surfaces, NLFD predicts unreasonable pressure distribution on both surfaces around shock positions.

Figure 10 indicates pressure distribution for the case run by CFD software at various arbitrary time instances. The results obtained by this software show that a moving shock occurs only on the upper surface. As can be seen, NLFD method can predict reasonable pressure distribution on the lower surface and results agree well with those of the CFD software. However, pressure distribution around shock positions on the upper cannot be predicted well.

Although NLFD predicts incorrect pressure distribution around shock positions, however, Figures 8-10 shows that pressure distributions away from shock positions

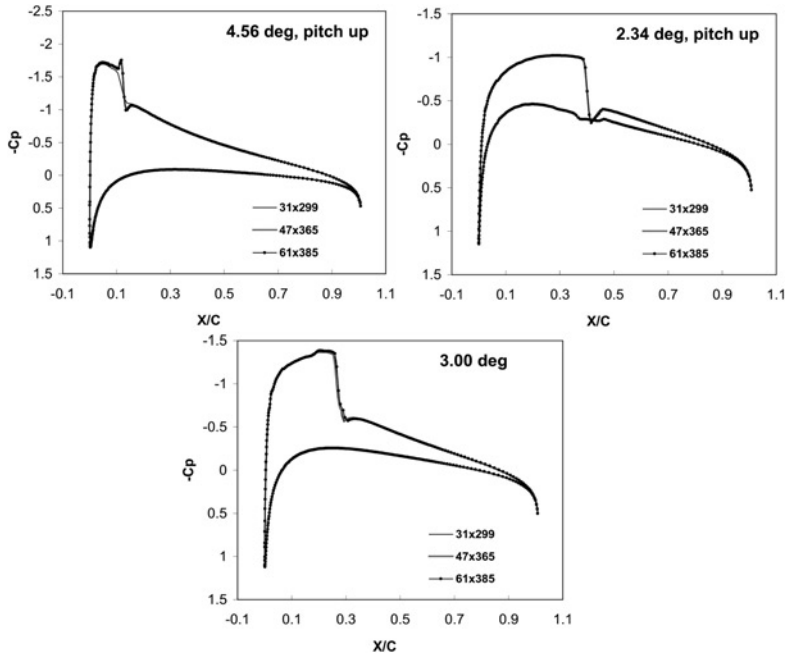

Figure 6.
Grid study for CT1 (top left), CT5 (top right) and the third (bottom) test case using five harmonics

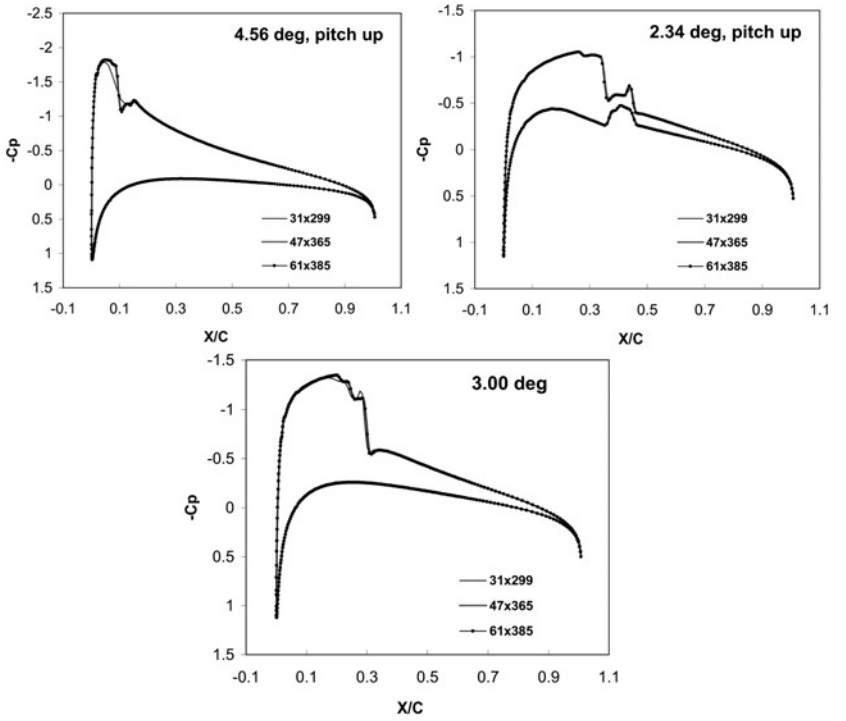

Figure 7.
Grid study for CT1 (top left), CT5 (top right) and the third (bottom) test case using seven harmonics

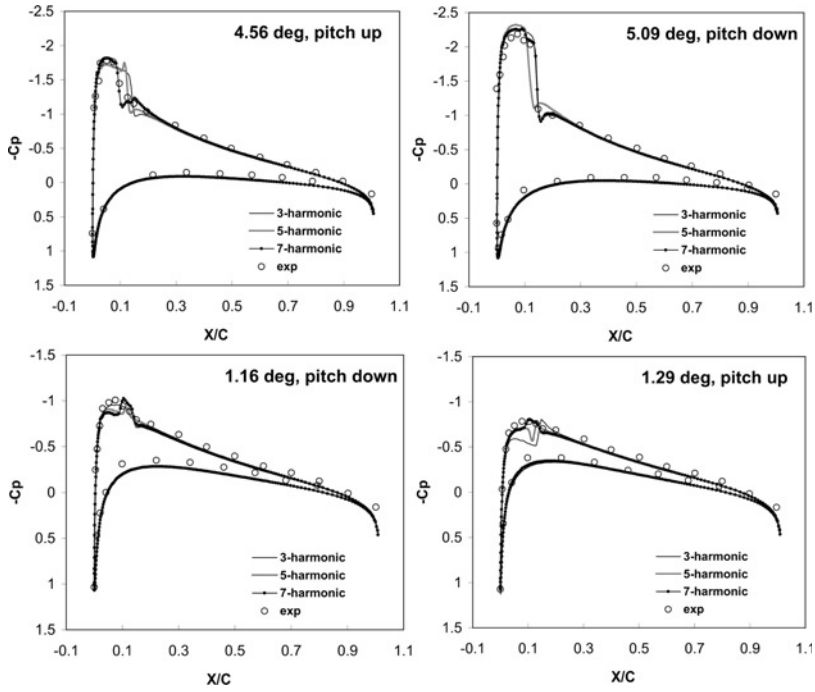

Figure 8.
Pressure distribution for CT1 test case at various time instances

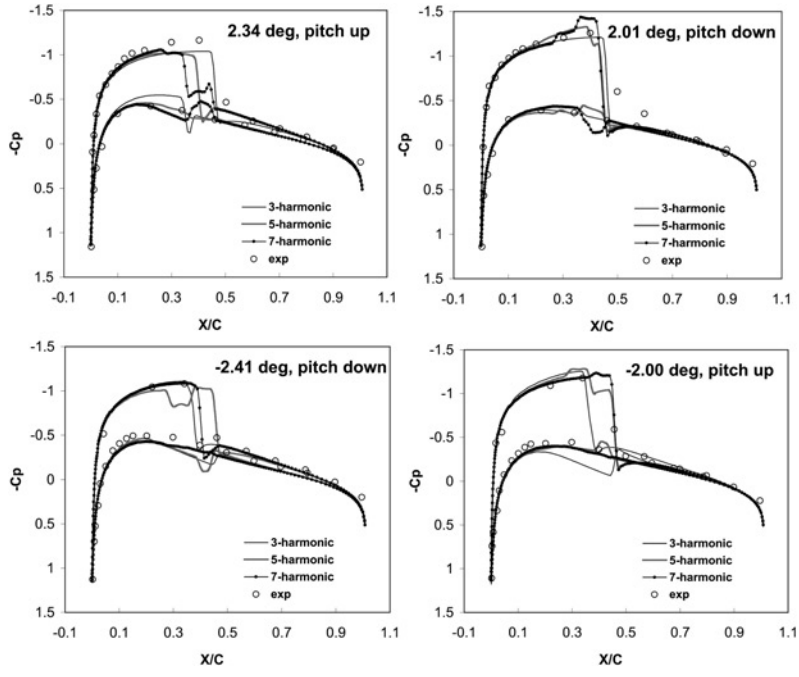

Figure 9.
Pressure distribution for CT5 test case at various time instances

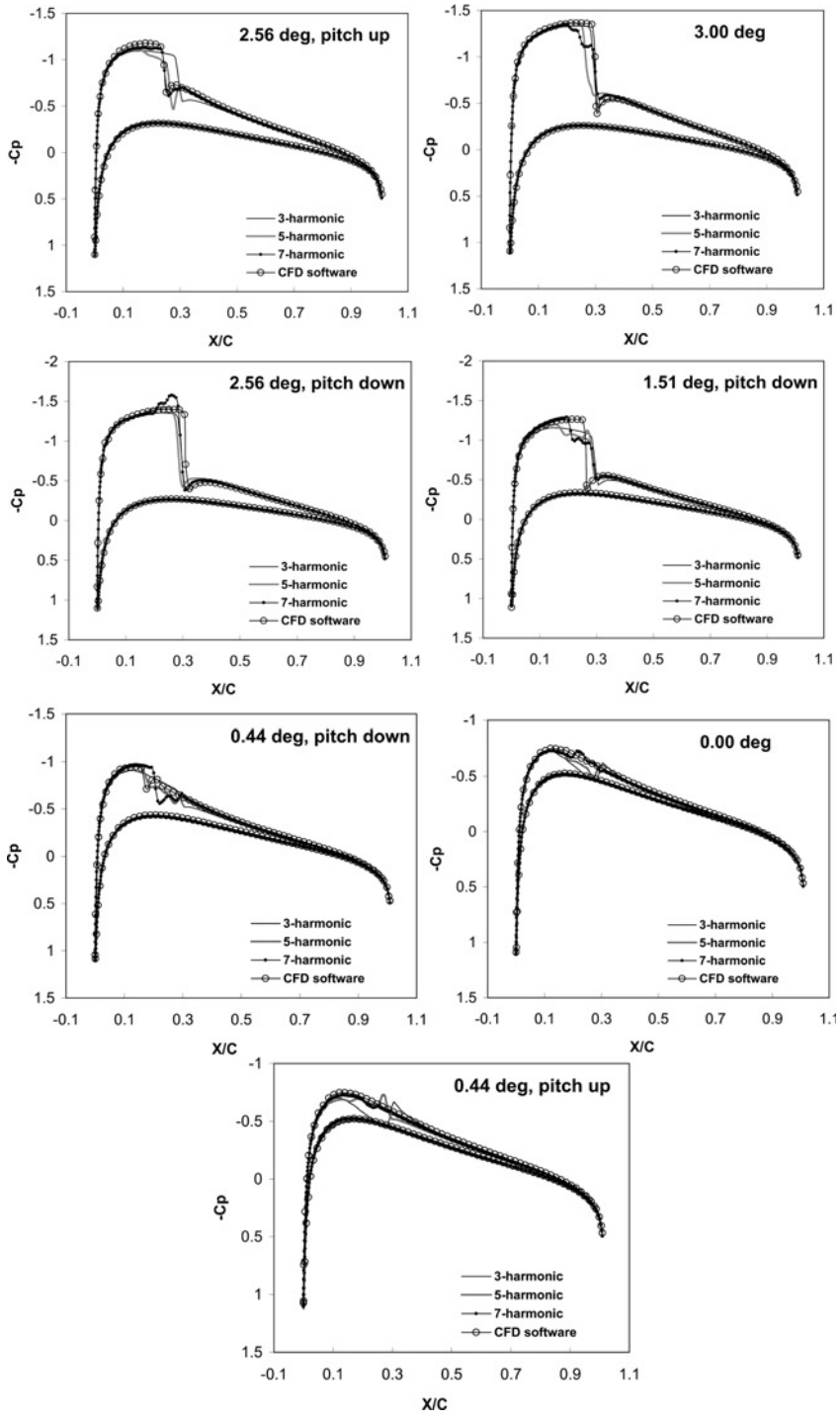

Figure 10.
Pressure distribution for the third case at various time instances

predicted by the NLFD method agree with those of the experiment or CFD software and little differences exist using three, five or seven harmonics.

Figure 11 presents normal force coefficient for CT1, CT5 and the third case vs incidence angle. Although there is undesirable pressure distribution around shock positions on the surface in which moving shock occurs, calculated normal forces are in good agreement with the experimental or CFD software results. There are also little differences between results using three, five or seven harmonics.

Although no convergence acceleration techniques are used in this research, however a comparative study regarding required computational time between the NLFD method and CFD software that is considered as a time accurate solver shows that the NLFD method with a low number of harmonic needs less computational time. The NLFD method is amenable to many convergence acceleration techniques used for

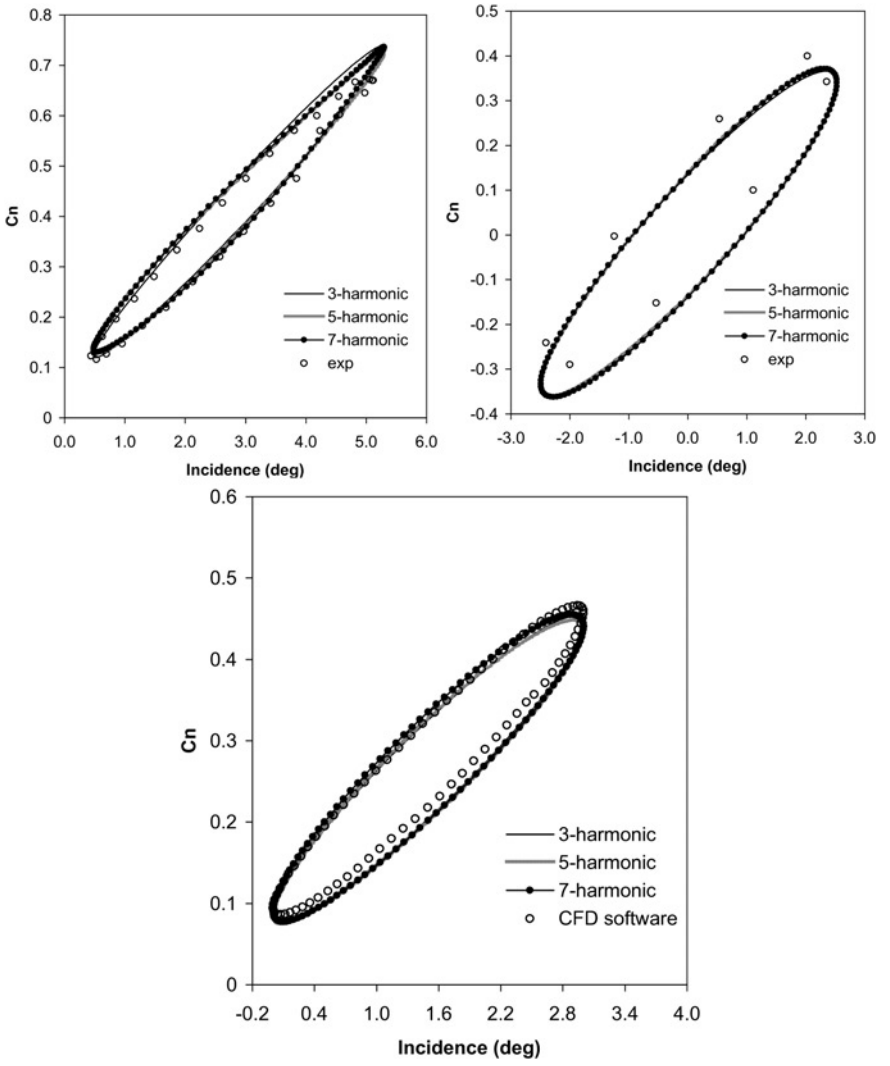

Figure 11.
Normal force coefficient for CT1 (top left), CT5 (top right) and third (bottom) test cases using different number of harmonics

steady-state flows. Using these techniques, better efficiency concerning computational time can be obtained, so this method would be more efficient than time accurate methods (McMullen and Jameson, 2006).

9. Conclusion

In this research, the capability of NLFD method in predicting details of unsteady transonic flow fields is investigated. Surface pressure coefficients in the time domain on pitching airfoils at three specified reduced frequency are presented. In the studied cases, at most seven harmonics are considered. Grid independency studies also show that the presented pressure distributions are mesh independent. Results show that NLFD method can predict reasonable pressure distribution in the time domain except in vicinity of moving shock positions with a few numbers of harmonics. Although this method takes less computational time compared to the conventional time accurate methods and gives accurate estimates of global properties such as lift coefficients, however unfair pressure distributions in the time domain may be predicted by the NLFD method around shock positions. This inaccurate pressure coefficient close to the shock positions is mainly due to high nonlinear effects introduced by shock wave. It is also shown that good pressure distributions in the time domain are predicted away from shock positions with only a few numbers of harmonics.

References

Adamczyk, J.J. (1984), "Model equation for simulating flows in multistage turbomachinery", NASA Technical Memorandum, NASA, Washington, DC.

Clark, W. (1992), "Prediction of unsteady flows in turbomachinery using the linearized Euler equations on deforming grids", master's thesis, Duke University, Durham, NC.

Hall, K.C. and Clark, W.S. (1993), "Linearized Euler predictions of unsteady aerodynamic loads in cascades", *AIAA Journal*, Vol. 31 No. 3, pp. 540-50.

Hall, K.C. and Crawley, E.F. (1989), "Calculation of unsteady flows in turbomachinery using the linearized Euler equations", *AIAA Journal*, Vol. 27 No. 6, pp. 777-87.

Hall, K.C. and Lorence, C.B. (1993), "Calculation of three dimensional unsteady flows in turbomachinery using the linearized harmonic Euler equations", *Transaction of ASME, Journal of Turbomachinery*, Vol. 115, pp. 800-9.

Hall, K.C., Clark, W.S. and Lorence, C.B. (1994), "A linearized Euler analysis of unsteady transonic flows in turbomachinery", *Transactions of ASME, Journal of Turbomachinery*, Vol. 116, pp. 477-88.

Hall, K.C., Thomas, J.P. and Clark, W.S. (2000), "Computation of unsteady nonlinear flows in cascades using a harmonic balance technique", *Proceedings of the 9th International Symposium on Unsteady Aerodynamics, Aeroacoustics and Aeroelasticity of Turbomachines, Lyon, 4-8 September*.

Hall, K.C., Thomas, J.P. and Clark, W.S. (2002), "Computation of unsteady nonlinear flows in cascades using a harmonic balance technique", *AIAA Journal*, Vol. 40 No. 5, pp. 879-86.

Holmes, D.G. and Chuang, H.A. (1993), "2D linearized harmonic Euler flow analysis for flutter and forced response", in Atassi, H.M. (Ed.), *Unsteady Aerodynamics, Aeroacoustics, and Aeroelasticity of Turbomachines and Propellers*, Springer-Verlag, New York, NY.

Landon, R.H. (2000), "NACA0012 oscillatory and transient pitching", Verification and Validation Data for Computational Unsteady Aerodynamics, RTO-TR-26, NATO Research and Technology Organisation, NATO, Brussels.

McMullen, M., Jameson, A. and Alonso, J. (2001), "Acceleration of convergence to a periodic steady state in turbomachinery flows", AIAA Paper No. 01-0152, *Proceedings of the AIAA 39th Aerospace Sciences Meeting, Reno, NV, January 8-11*.

McMullen, M., Jameson, A. and Alonso, J. (2002), "Application of a nonlinear frequency domain solver to the Euler and Navier-Stokes equations", AIAA Paper No. 02-0120, *Proceedings of the AIAA 40th Aerospace Sciences Meeting, Reno, NV, January 14-17*.

McMullen, M.S. (2003), "The application of non-linear frequency domain methods to the Euler and Navier-Stokes equations", PhD dissertation, Stanford University, Stanford, CA.

McMullen, M.S. and Jameson, A. (2006), "The computational efficiency of non-linear frequency domain methods", *Journal of Computational Physics*, Vol. 212, pp. 637-61.

Ni, R.H. and Sisto, F. (1976), "Numerical computation of nonstationary aerodynamics of flat plate cascades in compressible flow", *Transactions of the ASME, Journal of Engineering for Power*, Vol. 98, pp. 165-70.

Ning, W. and He, L. (1998), "Computation of unsteady flows around oscillating blades using linear and non-linear harmonic Euler methods", *Journal of Turbomachinery*, Vol. 120 No. 3, pp. 508-14.

Thomas, P., Dowell, E.H. and Hall, K.C. (2002), "Nonlinear inviscid aerodynamic effects on transonic divergence, flutter and limit cycle oscillations", *AIAA Journal*, Vol. 40 No. 4, pp. 638-46.

Uygun, M. and Kirkkopru, K. (2007), "Numerical solution of unsteady compressible flows on moving grids using dual time stepping", *Proceedings of the Ankara International Aerospace Conference, METU, Ankara, 10-12 September*.

Corresponding author
H. Emdad can be contacted at: hemdad@shirazu.ac.ir